# Determination of the true congruent composition for LiTaO3 single crystals using the LFB ultrasonic material characterization system



| | |
|---|---|
| 著者 | 櫛引 淳一 |
| journal or publication title | IEEE Transactions on Ultrasonics, Ferroelectrics and Frequency Control |
| volume | 53 |
| number | 2 |
| page range | 385-392 |
| year | 2006 |
| URL | http://hdl.handle.net/10097/46552 |

doi: 10.1109/TUFFC.2006.1593377

# Determination of the True Congruent Composition for $LiTaO_3$ Single Crystals Using the LFB Ultrasonic Material Characterization System

Jun-ichi Kushibiki, , and Yuji Ohashi,

***Abstract*—The true congruent composition for $LiTaO_3$ single crystals was determined by measuring the velocities of leaky surface acoustic waves (LSAWs) with the line-focus-beam ultrasonic material characterization (LFB-UMC) system for two $42°YX$-$LiTaO_3$ crystal ingots. The congruent composition determined here was 48.460 $Li_2O$-mol%, corresponding to the LSAW velocity ($42°YX$-$LiTaO_3$) of 3125.3 m/s, and the absolute relationship between the LSAW velocity and chemical composition was obtained. Simulations on the variation of the melt and crystal compositions in a mass production of 100 crystals were conducted as a function of the composition of the starting material around the congruent composition. The result showed that the distributions of the melt and crystal compositions within and among the crystals varied largely with the material composition, providing the relationship of the material composition with the maximum composition variation for the 100 crystals. Based on these results, we verified the relationships between the tolerance of the material composition variation and the tolerances for the SH-type SAW velocity, LSAW velocity, and Curie temperature. The material composition needs to be constrained to within $\pm 0.007$ $Li_2O$-mol% around the congruent composition to mass-produce the crystals with reliable homogeneity, satisfying the tolerance of $\pm 0.01\%$ in the SAW velocity. Furthermore, a guideline for the specification of reliable piezoelectric SAW-device wafer substrates was presented with the accurate interrelationships among the chemical composition ratio, LSAW velocity, and Curie temperature.**

## I. Introduction

Much research has been conducted on $LiTaO_3$ crystal growth by the Czochralski method [1]–[6] for application not only to surface acoustic wave (SAW) devices [7]–[11] but also to optoelectronic devices [12]–[15]. Homogeneity of the crystal substrates is necessary for mass-producing SAW devices with superior characteristics, but the quality is currently unsatisfactory for manufacturers of SAW devices. The basic problem is that the congruent composition has not yet been established. In particular, the mass-production process of growing a series of crystals in the same furnace and crucible includes steps such as adding the volume of the reduced $LiTaO_3$ material to the remaining melt in the crucible and growing the next crystal. When the melt composition is shifted from the congruent composition, the compositional distributions within and among the grown crystals are increased as the crystal growths are repeated [16]. In our previous research, we clarified, using the line-focus-beam ultrasonic material characterization (LFB-UMC) system [17], [18], that almost all crystal manufacturers have been producing crystals with some significant distributions in the chemical compositions. The distributions result from their growing crystals with chemical composition ratios differing from the congruent composition [19]–[21].

Another problem is the technology of evaluating the crystals. Manufacturers of the crystals and SAW devices most commonly conduct Curie temperature ($T_C$) measurements for evaluating the chemical compositions using thermal analysis methods. However, we have verified that the $T_C$ measurement is not sufficiently accurate and that temperature differences of 4°C maximum occur due to different measurement instruments or conditions [21]. This makes the measured $T_C$ values unreliable for evaluation. Thus, it is difficult to precisely determine the congruent composition by measuring $T_C$. Also, we should reconsider the $T_C$ specification for $LiTaO_3$ wafers for SAW devices (598 to 608) $\pm$ 3°C, that were not specifically determined [22].

Our accurate measurements of the velocity of leaky surface acoustic waves (LSAWs), $V_{LSAW}$, on a water-loaded specimen surface revealed that the variations of chemical compositions in grown crystals eventually are dominated mainly by the composition of the starting material. This is true regardless of other conditions when growing crystals, such as temperature distribution in the furnace, the rotating speed, and the pulling speed of crystals from the melts in a crucible. In fact, homogeneity of optical-grade $LiTaO_3$ single crystals has been improved using different compositions of the starting material determined by this system, resulting in the successful growth of crystals with higher homogeneity in LSAW velocity, i.e., chemical composition ratio [23]. The experiment suggested that further experiments should be conducted to obtain a precise value of the congruent composition.

Manuscript received January 4, 2005; accepted August 19, 2005. This work was supported in part by the Research Grant-in-Aid for the 21st COE (Center of Excellence) Program funded by the Japanese Ministry of Education, Culture, Sports, Science, and Technology.

The authors are with the Department of Electrical Engineering, Tohoku University, Sendai 980-8579, Japan (e-mail: kushi@ecei.tohoku.ac.jp).

In this paper, we determine the true congruent composition through $V_{\mathrm{LSAW}}$ measurements for 42°$Y$-cut $X$-propagating (42°$YX$-) $LiTaO_3$ [24] to grow much more homogeneous $LiTaO_3$ crystals in chemical composition. We first simulated compositional distributions within and among grown crystals in the $LiTaO_3$ crystal mass-production process with reference to the congruent composition determined, then estimated the variation tolerance of the starting material composition required to achieve the desired range. We subsequently determined more reliable relationships among the chemical composition ratio, $V_{\mathrm{LSAW}}$, and $T_{\mathrm{C}}$.

## II. Experiments

The measurement principle of the LFB-UMC system has been explained in detail in the literature [17]. The most recent system used in this study attained relative measurement accuracies of ±0.0013% in $V_{\mathrm{LSAW}}$ at an arbitrarily chosen single point on a specimen surface, and of ±0.003% over a two-dimensional scanning area of 75 mm × 75 mm [18], [20]. The absolute accuracy of $V_{\mathrm{LSAW}}$ was ±0.01% [25]–[27] after system calibration using the $LiTaO_3$ standard specimen [28], [29].

All specimen substrates used in the following experiments are only 0.35 mm thick, so the waves reflected from the back surface of the specimens can influence the $V_{\mathrm{LSAW}}$ measurements. We remove this influence by moving average processing for measured frequency dependences of $V_{\mathrm{LSAW}}$ [30].

From results in the literature [23], the true congruent composition was speculated to be about 48.47 $Li_2O$-mol%. Therefore, we first prepared two $LiTaO_3$ single crystals for SH-type SAW devices, grown along the 42°$Y$-axis direction with $Li_2O$ concentrations of 48.459 and 48.469 mol% as starting materials. The 42°$Y$-cut wafer specimens then were sliced at the top and bottom parts of each crystal ingot. Fig. 1 depicts the measured results of $V_{\mathrm{LSAW}}$ propagating along the $X$ axis (42°$YX$) with the LFB-UMC system at five measurement points at 10-mm intervals over a range of ±20 mm on each wafer specimen. Fig. 2 presents the straight lines for the results of averaged values of $V_{\mathrm{LSAW}}$ measured at the five measurement points on the surface of the specimens at the top and bottom parts of the two crystals, as a function of the $Li_2O$ concentration of the starting material. Here, the positions of the wafer specimens extracted for each crystal differed, so we plotted the respective values of $V_{\mathrm{LSAW}}$ estimated at two positions (0 mm and 118 mm) from the top of the crystal using a linear interpolation method. The $Li_2O$ concentration of the starting material (i.e., the congruent composition) was 48.460 mol% at the intersection of the two straight lines. We also can derive a corresponding LSAW velocity of 3125.3 m/s for 42°$YX$ $LiTaO_3$ in the true congruent composition. The $V_{\mathrm{LSAW}}$ gradient along the pulling direction became zero at the congruent composition of 48.460 $Li_2O$-mol%.

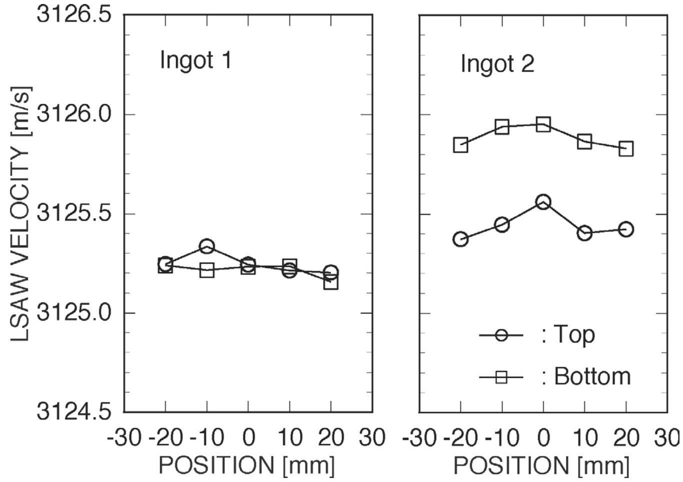


Fig. 1. LSAW velocity distributions measured for 42° -$LiTaO_3$ wafers prepared from tops and bottoms of two crystal ingots with melt compositions of 48.459 $Li_2O$-mol% for ingot 1 and 48.469 $Li_2O$-mol% for ingot 2.

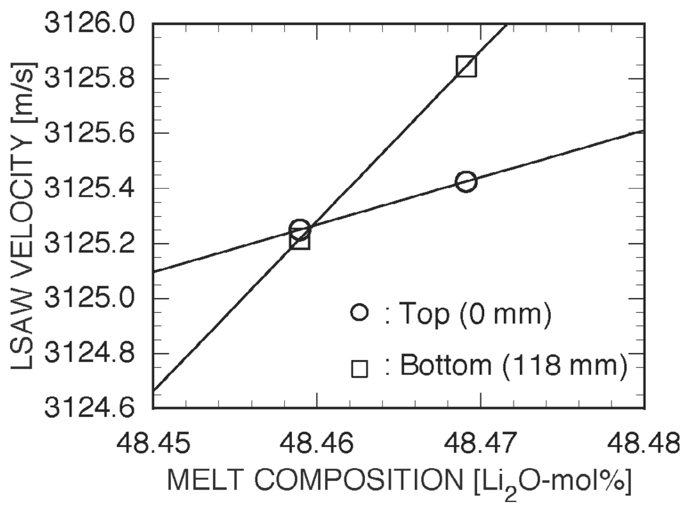


Fig. 2. Estimation of true congruent composition from the relationship between melt compositions and LSAW velocities at crystal top and bottom.

## III. Discussion

The material for a melt is obtained by sintering well-mixed powder material of $Li_2CO_3$ and $Ta_2O_5$, separately measured and compounded. Because $CO_2$ is evaporated during the sintering, the sintered material is a mixed material of $Li_2O$ and $Ta_2O_5$. Here we simulated a series of 100 crystal ingots consecutively mass produced with con-

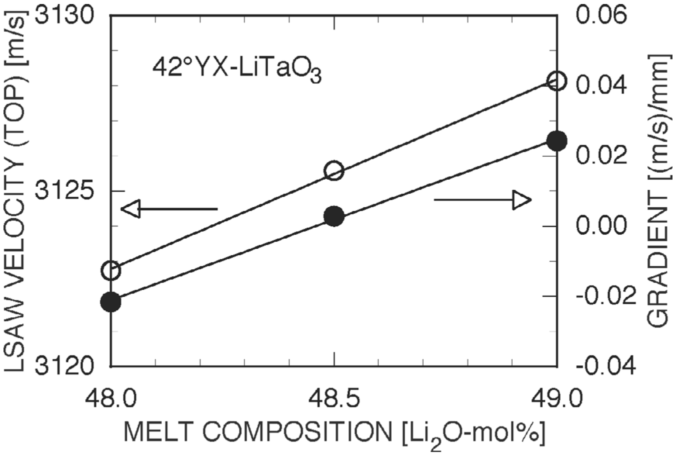


Fig. 3. LSAW velocities for 42° -$LiTaO_3$ prepared from the top of the grown crystals and gradients of LSAW velocities along the pulling-axis direction as a function of melt composition.

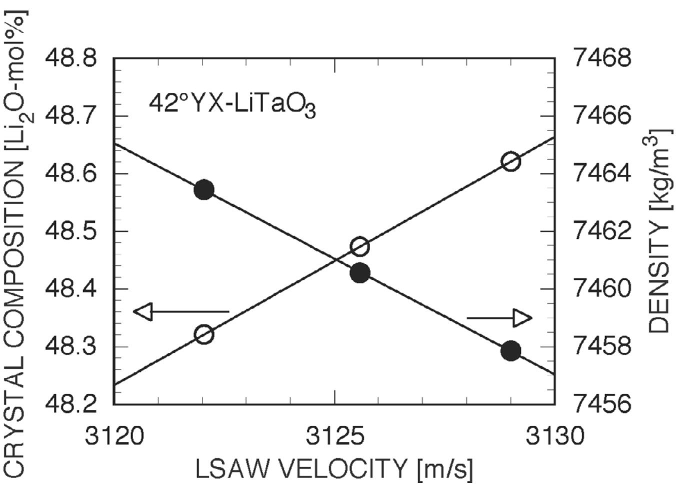


Fig. 4. Chemical compositions and densities as a function of LSAW velocity for 42° -$LiTaO_3$.

stant composition of the starting material, as a function of the composition around the true congruent composition of 48.460 $Li_2O$-mol%, assuming no recycled $LiTaO_3$ material.

We need to obtain the relationships among $V_{LSAW}$, melt composition, crystal composition, and density in advance as basic data for simulation. Here, SH-type 42°$YX$-$LiTaO_3$ substrates are considered. Fig. 3 illustrates the relationship between the melt compositions and $V_{LSAW}$ at the top of the grown crystals and the relationship between the melt compositions and $V_{LSAW}$ gradients along the pulling axis of the grown crystals. Fig. 4 illustrates the relationship between $V_{LSAW}$ and crystal compositions and the relationship between $V_{LSAW}$ and crystal densities. These results were obtained using the dependence data of the acoustical physical constants on the chemical composition ratios reported in [29] and the data of the $V_{LSAW}$ gradients along the pulling axis as well [28]. However, the absolute values in the chemical composition ratio were corrected so that the congruent composition was 48.460 $Li_2O$-mol% as determined in Section II-B. The data of the acoustical physical constants of $LiTaO_3$ at the congruent composition and their chemical composition dependences are presented in Table I.

TABLE I
Acoustical Physical Constants of $LiTaO_3$ Crystals at the Congruent Composition and their Chemical Composition Dependences.

| | | Constants at 48.460 $Li_2O$-mol% | Gradient (/mol%) |
|---|---|---|---|
| Elastic | $^{E}_{11}$ | 2.3296 | 0.023 |
| constant | $^{E}_{12}$ | 0.4638 | 0.011 |
| ($\times 10^{11}$ N/m$^2$) | $^{E}_{13}$ | 0.8352 | 0.000 |
| | $^{E}_{14}$ | −0.1065 | 0.008 |
| | $^{E}_{33}$ | 2.7569 | 0.028 |
| | $^{E}_{44}$ | 0.9516 | 0.002 |
| Piezoelectric | 15 | 2.630 | 0.135 |
| constant | 22 | 1.828 | 0.086 |
| (C/m$^2$) | 31 | −0.117 | 0.096 |
| | 33 | 1.793 | −0.082 |
| Dielectric | $^{S}_{11}$ 0 | 41.7 | 0.00 |
| constant | $^{S}_{33}$ 0 | 41.7 | −1.73 |
| Density (kg/m$^3$) | | 7460.8 | −18.61 |

We conducted numerical simulations on the mass-production process of the crystals using the relationships of Figs. 3 and 4. We assumed that the total weight of the material charged in a crucible for crystal growth is fixed, and that the grown crystals have a completely cylindrical shape and a constant diameter of $2r$. In addition, compositional distribution within each crystal is presumed not to be in the diameter direction, but to arise linearly only along the pulling axis. The influence from differences between the compositions of seed crystals and grown crystals on the crystal growth is not particularly considered here.

Fig. 5 illustrates the crystal growth processes. The $Li_2O$ concentration in the charge material composition, $P(Li_2O)$, is determined. Next, the $Li_2O$ concentration in the melt composition at the $n$-th crystal growth, $M(n)$, obtained by adding the charge material to the material remaining in the crucible after the previous crystal growth, is determined. For the first charge ($n = 1$), the material composition is assumed to be the melt composition. The LSAW velocity as a function of distance $x$ from the top ($x = 0$) of the crystal grown with $M(n)$, $V_{LSAW}(n, M(n); x)$, is defined in the following equation, using the LSAW velocity $V_{LSAW}(n, M(n); 0)$ at $x = 0$ and the $V_{LSAW}$ gradient along the pulling axis, $\Delta V_{LSAW}(n, M(n))$, obtained in Fig. 3:

$$V_{LSAW}(n, M(n); x) = V_{LSAW}(n, M(n); 0) + x \times \Delta V_{LSAW}(n, M(n)). \quad (1)$$

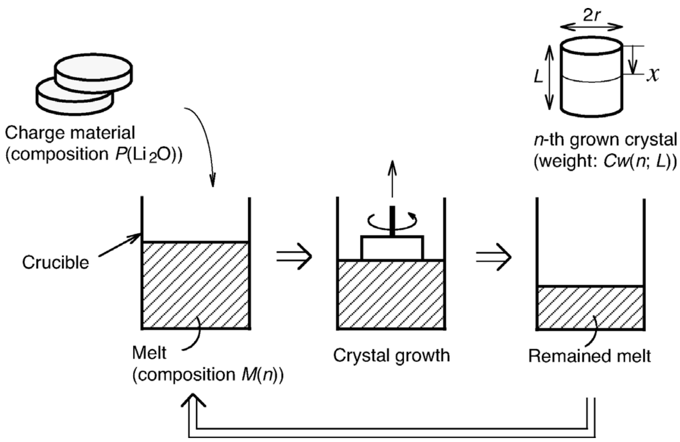


Fig. 5. A schematic of mass-producing crystals for simulations.

$V_{\mathrm{LSAW}}(n, M(n); x)$ obtained in (1) is converted into the crystal composition $C(n, M(n); x)$ and density $\rho(n, M(n); x)$, using the relationships of Fig. 4. The length of the grown crystal, $x = L$, is determined when the crystal weight $Cw(n; L)$ expressed as (2) corresponds to the solidification percentage (i.e., ratio of the weight of the grown crystal to the total weight of the material charged in the crucible):

$$Cw(n; L) = \int_0^L \pi r^2 \times \rho(n, M(n); x) dx. \qquad (2)$$

When the molecular weights of $Li_2O$ and $Ta_2O_5$ are represented as $W(Li_2O)$ and $W(Ta_2O_5)$, the rate of $Li_2O$ weight to the crystal weight at $x$, $R(n, M(n); x)$, is expressed by (3) (see next page).

Material weights of $Cw(Li_2O; n; L)$ and $Cw(Ta_2O_5; n; L)$ for $Li_2O$ and $Ta_2O_5$ of the crystal weight $Cw(n; L)$ for the crystal length $L$ is are obtained by the following equations:

$$Cw\,(Li_2O; n; L) = \int_0^L \pi r^2 \times \rho(n, M(n); x) \times R(n, M(n); x) dx \qquad (4)$$

$$Cw\,(Ta_2O_5; n; L) = Cw(n; L) - Cw\,(Li_2O; n; L). \qquad (5)$$

Material weights of $Mw(Li_2O; n; L)$ and $Mw(Ta_2O_5; n; L)$ remaining in the crucible are obtained by separately subtracting material weights of $Cw(Li_2O; n; L)$ and $Cw(Ta_2O_5; n; L)$ obtained with (4) and (5) from material weights of $Li_2O$ and $Ta_2O_5$ contained in the melt, $Mw(Li_2O; n)$ and $Mw(Ta_2O_5; n)$, when starting crystal growth. We determine each material weight of $Li_2O$ and $Ta_2O_5$, $Mw(Li_2O; n+1)$ and $Mw(Ta_2O_5; n+1)$, when the charge material [composition $P(Li_2O)$] with the same weight as the crystal weight $Cw(n; L)$ obtained by (2) is added to the remaining melt. This melt composition is set as the melt composition $M(n+1)$ for the next crystal growth, and the above calculation steps are repeated.

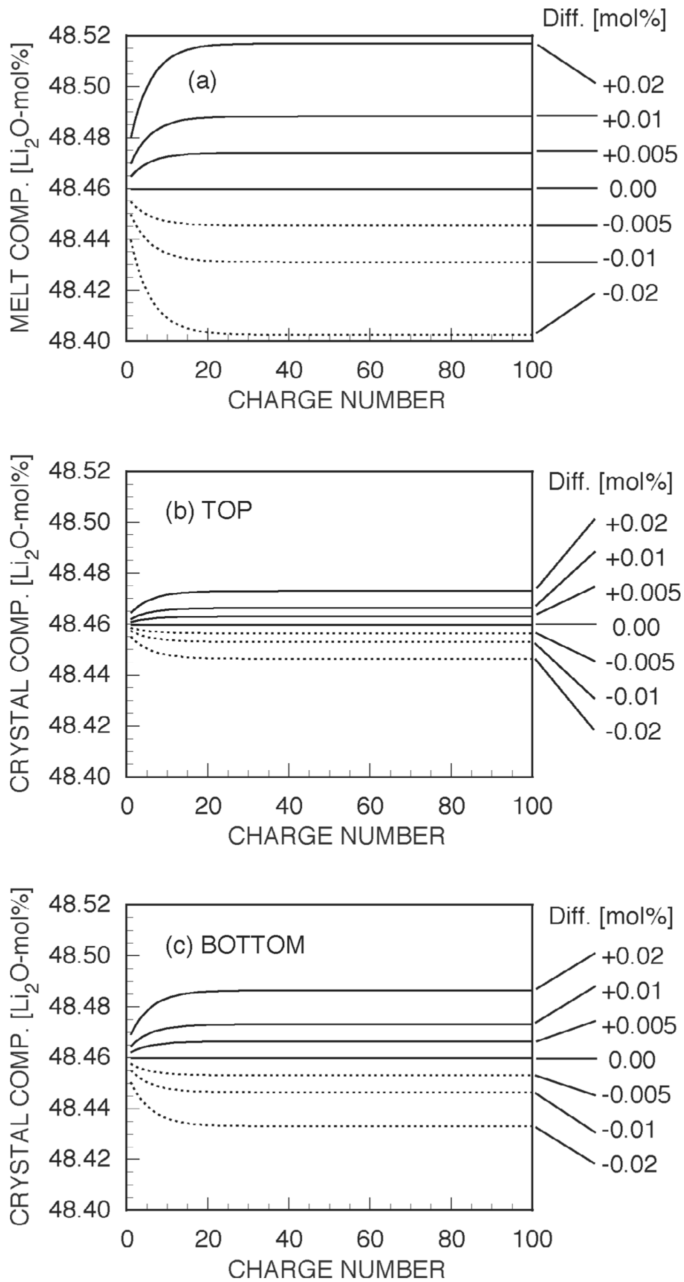


Fig. 6. Charge number dependence of chemical compositions for the melt (a), and for the crystals grown at the top (b) and at bottom (c), obtained for simulation of 100 consecutive crystal growths with parameters differing from the congruent composition.

Simulations were conducted as a function of the charge material composition for 100 repeated crystal growths, according to the above procedure. The assumptions are that cylindrical crystals are grown with a total weight of the starting material (melt) of 8200 g, solidification percentage of 50% (4100 g), and diameter of 77 mm. The charge material compositions also are assumed, just shifted at 0, ±0.005, ±0.01, and ±0.02 $Li_2O$-mol% from the congruent composition of 48.460 $Li_2O$-mol%. Fig. 6 presents the results of dependences of the charge number on the melt composition and the crystal compositions at the crystal top (0 mm) and bottom (118 mm). When the charge ma-

$$R(n, M(n); x) = \frac{W\,(\mathrm{Li_2O}) \times C(n, M(n); x)}{W\,(\mathrm{Li_2O}) \times C(n, M(n); x) + W\,(\mathrm{Ta_2O_5}) \times \{100 - C(n, M(n); x)\}}. \quad (3)$$

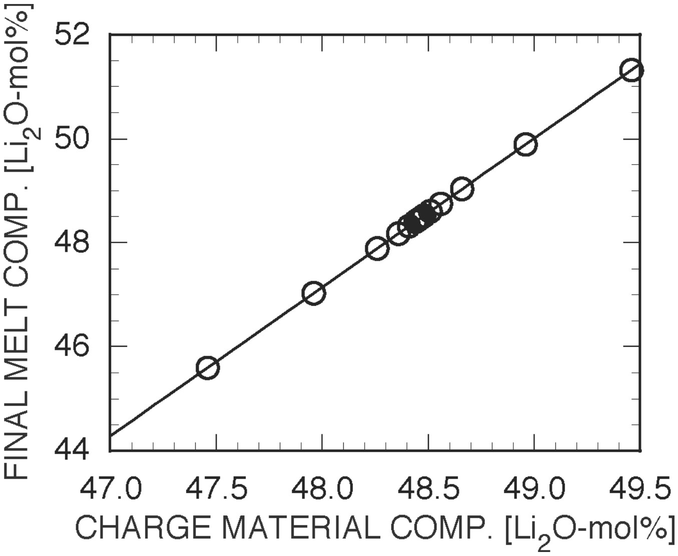


Fig. 7. Relationship between chemical compositions of the charge materials and the final saturated melt.

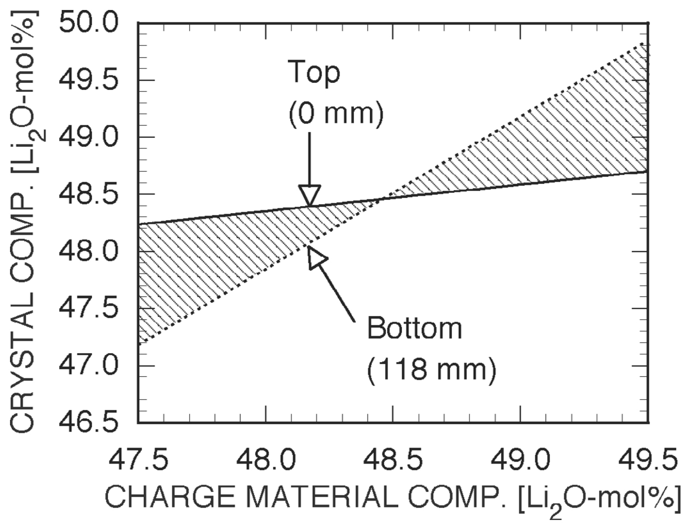


Fig. 8. Relationship between charge material compositions and maximum composition variations of the grown crystals. Solid line: compositions at the top of the first-crystal. Dotted line, compositions at the bottom of the 100th crystal. Slashed area, variation area in crystal composition for 100 crystal ingots grown with each charge material composition.

terial composition $P(\mathrm{Li_2O})$ is equal to the congruent composition, neither the melt nor crystal compositions vary, even after 100 consecutive crystals are grown. However, as the $P(\mathrm{Li_2O})$ departs from the congruent composition, the variations of the melt and crystal compositions become larger. The variations increase (or decrease) monotonically until the 20th charge, after which the variations are saturated. The relationship between the charge material composition and the melt composition at the saturation point (100th charge) is depicted in Fig. 7. The approximated line in Fig. 7 was obtained by the least-squares method, including the calculation results when the charge material composition is shifted by ±0.5, ±1.0 $\mathrm{Li_2O}$-mol% from the congruent composition, in addition to the result of Fig. 6(a).

We now discuss tolerances in the melt composition of the starting material to keep compositional distributions among crystal ingots within a desired range. When the charge material composition varies from the congruent composition, the maximum composition variation among the crystals grown from the first charge to the 100th charge can be obtained by the difference between the two compositions at the top of the crystal grown by the first charge and at the bottom of the crystal grown by the 100th charge. The compositions are obtained as a function of the charge material composition from Figs. 6(b) and (c), and the results are presented in Fig. 8. The slashed area in Fig. 8 represents the variation in the crystal composition for the 100 crystal ingots pulled with each charge material composition. The relationship of this maximum composition variation $\Delta C_{\mathrm{MAX}}$ and the charge material composition $P(\mathrm{Li_2O})$ is expressed by the following equation:

$$\Delta C_{\mathrm{MAX}} = 1.101 \times (P\,(\mathrm{Li_2O}) - 48.460)\,. \quad (6)$$

We assume the tolerances to be ±0.1%, ±0.05%, ±0.02%, ±0.01%, ±0.005%, and ±0.002% in the SH-type SAW velocity ($V_{\mathrm{SAW}}$) for the 42°$YX$-$\mathrm{LiTaO_3}$ SAW device substrates. Table II presents the results obtained for variations of $V_{\mathrm{LSAW}}$, crystal composition, charge material composition, and $T_{\mathrm{C}}$, corresponding to the $V_{\mathrm{SAW}}$ tolerances. Here, the relationship between $V_{\mathrm{LSAW}}$ and $V_{\mathrm{SAW}}$ for the 42°$YX$-$\mathrm{LiTaO_3}$ substrates (Fig. 9) is obtained by calculations, using the acoustical physical constants in [29]. Growing crystals using the congruent composition determined above produces crystals with ideally homogeneity. However, experimental evidence obtained so far [16], [19]–[21], [23] verified that the $V_{\mathrm{LSAW}}$ distributions around ±0.01% along the diameter direction were observed independent of the starting material composition. Therefore, when a $V_{\mathrm{SAW}}$ tolerance variation of ±0.01% is taken for the wafer substrates, the material composition range should be defined as 48.460 ± 0.007 $\mathrm{Li_2O}$-mol%, the congruent composition for mass production. In this situation, crystals with a $T_{\mathrm{C}}$ variation of less than ±0.4°C can be mass produced, as compared to the $T_{\mathrm{C}}$ tolerance of ±3°C [22] determined as the current wafer specification for SAW devices.

TABLE II
TOLERANCES OF LSAW VELOCITY, CURIE TEMPERATURE, CRYSTAL COMPOSITION, AND CHARGE MATERIAL COMPOSITION CORRESPONDING TO TOLERANCE OF SH-TYPE SAW VELOCITY FOR 42° -$LiTaO_3$.

| | Congruent | Tolerance of SAW velocity | | | | | |
|---|---|---|---|---|---|---|---|
| | Comp. | ±0.1% | ±0.05% | ±0.02% | ±0.01% | ±0.005% | ±0.002% |
| SAW velocity [m/s] | 4213.49 | ±4.21 | ±2.11 | ±0.84 | ±0.42 | ±0.21 | ±0.08 |
| LSAW velocity [m/s] | 3125.26 | ±2.28 | ±1.14 | ±0.46 | ±0.23 | ±0.11 | ±0.05 |
| Curie temp. [°C] | 603.0 | ±3.82 | ±1.91 | ±0.76 | ±0.38 | ±0.19 | ±0.08 |
| Crystal comp. [$Li_2O$-mol%] | 48.460 | ±0.099 | ±0.049 | ±0.020 | ±0.010 | ±0.005 | ±0.002 |
| Material comp. [$Li_2O$-mol%] | 48.460 | ±0.074 | ±0.037 | ±0.015 | ±0.007 | ±0.004 | ±0.002 |

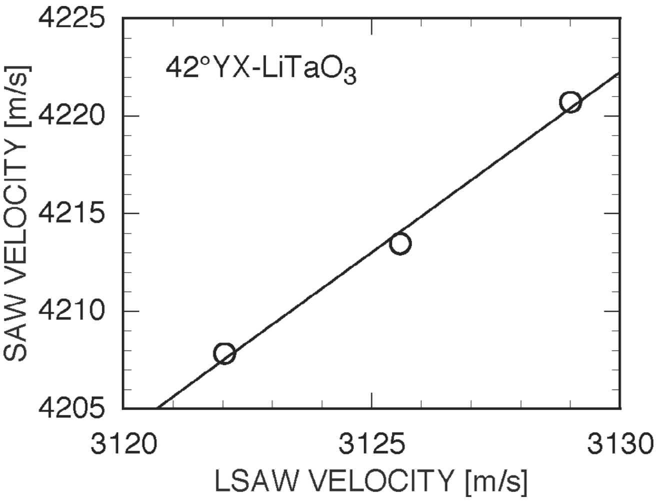


Fig. 9. Relationship between SH-type SAW velocities and Rayleigh-type LSAW velocities for 42° -$LiTaO_3$.

In the above simulations, we assumed that the charge material composition was constant for 100 crystal growths. However, we can consider two additional factors in actual mass production to discuss such slight variations of the crystal compositions: recycled $LiTaO_3$ used in the melt and measurement errors when weighing $Li_2CO_3$ and $Ta_2O_5$. Once the preferable composition is established, any recycled materials can be used in any charge, provided they remain within the maximum composition variations simulated above. Weight measurement errors might occur due to simple human errors or to errors from the moisture included in the powder, depending upon the ambient humidity. This implies there might be differences between the compositions expected at the starting material and the compositions of a sinter (or a melt) actually made. Controlling the environmental conditions of room temperature or humidity when weighing or preparing the chemical materials might ultimately lead to crystal growth with excellent homogeneity that cannot be evaluated with the conventional $T_C$ measurement accuracy. More efficient, lower cost mass production of crystals could be possible because the homogeneity in chemical composition would be fixed.

As mentioned, we obtained the absolute relationship of the chemical composition ratio with $V_{LSAW}$. We now can derive the relationships among other physical or chemical properties ($T_C$, $V_{SAW}$, and lattice constants of $a$ and $c$) and chemical composition ratios, using $V_{LSAW}$ as a standardized scale. Here, we determine the relationship of the chemical composition ratio with $T_C$ that is widely used to evaluate the chemical composition ratio.

In the literature [31], we investigated the proper measurement conditions for higher reproducibility and a calibration method for obtaining absolute values to ensure reliable $T_C$ measured values using a differential scanning calorimetry (DSC) system. We found that the relationship between $V_{LSAW}$ and $T_C$ for 42°$YX$-$LiTaO_3$ substrates is expressed by the following equation:

$$T_C = 1.68 \times (V_{LSAW} - 3125.3) + 603.0. \quad (7)$$

As seen from (7), $V_{LSAW}$ is 3125.3 m/s, corresponding to the congruent composition of 48.460 $Li_2O$-mol% for which $T_C$ is 603.0°C. The relationship of the LSAW velocity to the crystal composition $C(Li_2O)$ for 42°$YX$-$LiTaO_3$ substrates obtained in Fig. 4 is:

$$C\,(Li_2O) = 0.0433 \times (V_{LSAW} - 3125.3) + 48.460. \quad (8)$$

Using (7) and (8), the relationship between $C(Li_2O)$ and $T_C$ can be derived easily as follows:

$$C\,(Li_2O) = 0.0258 \times (T_C - 603.0) + 48.460. \quad (9)$$

Thus, $T_C$ of 603.0°C is specifically defined for the congruent composition (48.460 $Li_2O$-mol%), instead of the indefinite specification (598 to 608°C) for $T_C$ given in the literature [22].

## IV. Conclusions

We used the LFB-UMC system to determine the true congruent composition for $LiTaO_3$ crystals with excellent homogeneity by accurately measuring LSAW velocities for two 42°$YX$-$LiTaO_3$ crystals grown around the nearly congruent composition. We also obtained the absolute relationship between the LSAW velocity and chemical composition: the congruent composition was estimated to be 48.460 $Li_2O$-mol%, and the corresponding LSAW velocity (42°$YX$-$LiTaO_3$) was 3125.3 m/s. In addition, variations of the melt and crystal compositions (charge number dependence) were simulated, assuming the material composition shifted from the congruent composition for mass production of the crystals. The result demonstrated that the melt composition and the compositional distribution within and among the crystals vary significantly when the starting material composition differs from the congruent composition. However, the variation is remarkable until the 20th charge; thereafter, the compositional distributions saturate. This result led to a correlation of the maximum composition variation in the crystals with the starting material composition. Based on these results, we verified the relationships of the tolerance of the material composition variation with the tolerances for the SH-type SAW velocity, LSAW velocity, and Curie temperature. We must control the material composition variation within ±0.007 $Li_2O$-mol% for the congruent composition to mass produce the crystals required for a tolerance of ±0.01% in the SAW velocity. Furthermore, we proved the absolute relationships among the chemical composition ratio, LSAW velocity, and Curie temperature.

Mass producing $LiTaO_3$ crystals using the congruent composition determined in this paper should yield extremely small compositional distributions within and among the crystals. This will enable us to eliminate the conventional process of evaluating the chemical composition using $T_C$ and consequently to reduce the cost of producing substrates for fabricating SAW devices with higher performance. This paper will contribute to the establishment of the specifications for reliable piezoelectric SAW wafer substrates and to supplying those substrates.

## Acknowledgment

This work was supported in part by the Research Grant-in-Aid for the 21st Center of Excellence Program funded by the Japanese Ministry of Education, Culture, Sports, Science, and Technology.

## References

[1] A. A. Ballman, "Growth of piezoelectric and ferroelectric materials by the Czochralski technique," *J. Amer. Ceram. Soc.*, vol. 48, pp. 112–113, Feb. 1965.

[2] R. L. Barns and J. R. Carruthers, "Lithium tantalate single crystal stoichiometry," *J. Appl. Crystallogr.*, vol. 3, pp. 395–399, 1970.

[3] S. Miyazawa and H. Iwasaki, "Congruent melting composition of lithium metatantalate," *J. Cryst. Growth*, vol. 10, pp. 276–278, Aug. 1971.

[4] C. D. Brandle and D. C. Miller, "Czochralski growth of large diameter $LiTaO_3$ crystals," *J. Cryst. Growth*, vol. 24/25, pp. 432–436, Oct. 1974.

[5] T. Fukuda, S. Matsumura, H. Hirano, and T. Ito, "Growth of $LiTaO_3$ single crystal for SAW device applications," *J. Cryst. Growth*, vol. 46, pp. 179–184, Feb. 1979.

[6] S. Matsumura, "Growth conditions for large diameter X-axis $LiTaO_3$ crystals," *J. Cryst. Growth*, vol. 51, pp. 41–46, Jan. 1981.

[7] H. Hirano, T. Fukuda, S. Matsumura, and S. Takahashi, "$LiTaO_3$ single crystals for SAW device applications: 1. Characteristics of the material," in *Proc. 1st Meeting Ferroelect. Mater. Their Appl.*, 1977, pp. 81–86.

[8] K. Nakamura, M. Kazumi, and H. Shimizu, "SH-type and Rayleigh-type surface waves on rotated Y-cut $LiTaO_3$," in *Proc. IEEE Ultrason. Symp.*, 1977, pp. 819–822.

[9] K. Yamada, T. Omi, S. Matsumura, and T. Nishimura, "Characterization of 4-inch $LiTaO_3$ single crystals for SAW device application," in *Proc. IEEE Ultrason. Symp.*, 1984, pp. 243–248.

[10] M. Sato, A. Iwama, J. Yamada, M. Hikita, and Y. Furukawa, "SAW velocity variation $LiTaO_3$ substrates," *Jpn. J. Appl. Phys.*, vol. 28, Suppl. 28-1, pp. 111–113, 1989.

[11] K. Yamanouchi, "Surface acoustic wave devices," *IEICE Trans. Electron.*, vol. J82-C-I, pp. 689–696, Dec. 1999.

[12] K. Yamamoto, K. Mizuuchi, K. Takeshige, Y. Sasai, and T. Taniuchi, "Characteristics of periodically domain-inverted $LiNbO_3$ and $LiTaO_3$ waveguides for second harmonic generation," *J. Appl. Phys.*, vol. 70, pp. 1947–1951, Aug. 1991.

[13] H. Åhlfeldt, "Nonlinear optical properties of proton-exchanged waveguides in z-cut $LiTaO_3$," *J. Appl. Phys.*, vol. 76, pp. 3255–3260, Sep. 1994.

[14] K. S. Abedin, M. Sato, H. Ito, T. Maeda, K. Shimamura, and T. Fukuda, "Ordinary and extraordinary continuous wave lasing at 1.092 and 1.082 m in bulk Nd:$LiTaO_3$ crystal," *J. Appl. Phys.*, vol. 78, pp. 691–693, July 1995.

[15] Y. N. Korkishko, V. A. Fedorov, S. M. Kostritskii, A. N. Alkaev, E. I. Maslennikov, E. M. Paderin, D. V. Apraksin, and F. Laurell, "Proton exchanged $LiNbO_3$ and $LiTaO_3$ optical waveguides and integrated optic devices," *Microelectron. Eng.*, vol. 69, pp. 228–236, 2003.

[16] J. Kushibiki, Y. Ohashi, and Y. Ono, "Evaluation and selection of $LiNbO_3$ and $LiTaO_3$ substrates for SAW devices by the LFB ultrasonic material characterization system," *IEEE Trans. Ultrason., Ferroelect., Freq. Contr.*, vol. 47, pp. 1068–1076, July 2000.

[17] J. Kushibiki and N. Chubachi, "Material characterization by line-focus-beam acoustic microscope," *IEEE Trans. Sonics Ultrason.*, vol. SU-32, pp. 189–212, Mar. 1985.

[18] J. Kushibiki, Y. Ono, Y. Ohashi, and M. Arakawa, "Development of the line-focus-beam ultrasonic material characterization system," *IEEE Trans. Ultrason., Ferroelect., Freq. Contr.*, vol. 49, pp. 99–113, Jan. 2002.

[19] J. Kushibiki, Y. Ohashi, and M. Mochizuki, "Evaluation of mass-produced commercial $LiTaO_3$ single crystals using the LFB ultrasonic material characterization system," *IEEE Trans. Ultrason., Ferroelect., Freq. Contr.*, vol. 51, pp. 748–755, June 2004.

[20] J. Kushibiki, Y. Ohashi, and T. Ujiie, "Standardized evaluation of chemical compositions of $LiTaO_3$ single crystals for SAW devices using the LFB ultrasonic material characterization system," *IEEE Trans. Ultrason., Ferroelect., Freq. Contr.*, vol. 49, pp. 454–465, Apr. 2002.

[21] J. Kushibiki, Y. Ohashi, and N. Mishima, "Calibration of Curie temperatures for $LiTaO_3$ single crystals by the LFB ultrasonic material characterization system," *IEEE Trans. Ultrason., Ferroelect., Freq. Contr.*, vol. 50, pp. 544–552, May 2003.

[22] *IEC-PAS Single Crystal Wafers Applied for Surface Acoustic Wave Device—Specification and Measuring Method, IEICE/Standard-0002*, April 17, 2001.

[23] J. Kushibiki, Y. Ohashi, Y. Ono, and T. Sasamata, "Evaluation and improvement of optical-grade $LiTaO_3$ single crystals by the LFB ultrasonic material characterization system," *IEEE Trans. Ultrason., Ferroelect., Freq. Contr.*, vol. 49, pp. 905–914, July 2002.

[24] O. Kawachi, S. Mineyoshi, G. Endoh, M. Ueda, O. Ikata, K. Hashimoto, and M. Yamaguchi, "Optimum cut for leaky SAW on $LiTaO_3$ for high performance resonators and filters," *IEEE Trans. Ultrason., Ferroelect., Freq. Contr.*, vol. 48, pp. 1442–1448, Sep. 2001.

[25] J. Kushibiki and M. Arakawa, "A method for calibrating the line-focus-beam acoustic microscopy system," *IEEE Trans. Ultrason., Ferroelect., Freq. Contr.*, vol. 45, pp. 421–430, Mar. 1998.

[26] J. Kushibiki, M. Arakawa, and R. Okabe, "High-accuracy standard specimens for the line-focus-beam ultrasonic material characterization system," *IEEE Trans. Ultrason., Ferroelect., Freq. Contr.*, vol. 49, pp. 827–835, June 2002.

[27] Y. Ohashi and J. Kushibiki, "Development of an improved calibration method for the LFB ultrasonic material characterization system," *IEEE Trans. Ultrason., Ferroelect., Freq. Contr.*, vol. 51, pp. 686–694, June 2004.

[28] J. Kushibiki, T. Okuzawa, J. Hirohashi, and Y. Ohashi, "Line-focus-beam acoustic microscopy characterization of optical-grade $LiTaO_3$ single crystals," *J. Appl. Phys.*, vol. 87, pp. 4395–4403, May 2000.

[29] J. Kushibiki, I. Takanaga, S. Komatsuzaki, and T. Ujiie, "Chemical composition dependences of the acoustical physical constants of $LiNbO_3$ and $LiTaO_3$ single crystals," *J. Appl. Phys.*, vol. 91, pp. 6341–6349, May 2002.

[30] J. Kushibiki, Y. Ohashi, and M. Arakawa, "Influence of reflected waves from the back surface of thin solid-plate specimen on velocity measurements by line-focus-beam acoustic microscopy," *IEEE Trans. Ultrason., Ferroelect., Freq. Contr.*, vol. 47, pp. 274–284, Jan. 2000.

[31] J. Kushibiki, Y. Ohashi, and Y. Ogasawara, "Reliable Curie temperature measurements for chemical compositions of $LiTaO_3$ crystals for SAW devices," submitted for publication.

**Jun-ichi Kushibiki** (M'83) was born in Hirosaki, Japan, on November 23, 1947. He received the B.S., M.S., and Ph.D. degrees in electrical engineering from Tohoku University, Sendai, Japan, in 1971, 1973, and 1976, respectively.

In 1976 he became a research associate at the Research Institute of Electrical Communication, Tohoku University. In 1979, he joined the Department of Electrical Engineering, Faculty of Engineering, Tohoku University, where he was an associate professor from 1988 to 1993 and became a professor in 1994.

Dr. Kushibiki has been studying ultrasonic metrology, especially acoustic microscopy and its applications, and established a method of material characterization by line-focus-beam acoustic microscopy. He also has been interested in biological tissue characterization in the higher frequency range applying both bulk and acoustic microscopy techniques.

He is a Fellow of the Acoustical Society of America; a Member of the Institute of Electronics, Information and Communication Engineers of Japan, of the Institute of Electrical Engineers of Japan, of the Acoustical Society of Japan, and of the Japan Society of Ultrasonics in Medicine.

**Yuji Ohashi** (M'03) was born in Toyama prefecture, Japan, on August 27, 1973. He received the B.S., M.S., and Ph.D. degrees in electrical engineering from Tohoku University, Sendai, Japan, in 1996, 1999, and 2003, respectively.

In 2003 he became a Center of Excellence (COE) Fellow (Post Doctoral) at the Department of Electronics, Graduate School of Engineering, Tohoku University. His research interests include development of line-focus-beam acoustic microscopy system and its applications to materials characterization.

Dr. Ohashi is a member of the Acoustical Society of Japan.